MATERIALS CHEMISTRY FRONTIERS

REVIEW

View Article Online
View Journal | View Issue

Cite this: *Mater. Chem. Front.*, 2023, **7**, 3922

Construction of organic micro/nanocrystal lasers: from molecules to devices

Ying-Li Shi,†[a] Ling-Yi Ding,†[b] Yun Hu,[c] Qiang Lv,[b] Wan-Ying Yang[b] and Xue-Dong Wang *[b]

Received 27th April 2023,
Accepted 21st May 2023

DOI: 10.1039/d3qm00461a

rsc.li/frontiers-materials

The rapid development of integrated circuits from the electron tube to the transistor has made the electronic components in integrated circuits develop towards miniaturization, which results in the growing demand for micro/nanoscale solid-state lasers. Organic semiconductor materials are vital in various optoelectronic devices, such as field effect transistors, light-emitting diodes, and optical waveguides. Especially, the solid-state laser behavior of organic micro/nanocrystals relying on intermolecular interactions are expected to be promising candidates in constructing novel miniaturized electronics due to their adjustable physicochemical properties, tunable optical performance, and the built-in cavity for optical confinement. However, there are still many difficulties to overcome before organic crystals are actually served as components in integrated circuits. Herein, we summarize and look forward to the future development directions of organic micro/nanocrystal lasers.

1. Introduction

As an important tool of modern science and technology, lasers have been widely applied to information science, industry, medicine, national defense, and many other fields since laser oscillation in ruby was first reported sixty years ago.[1,2] At present, the research and application of various inorganic semiconductor lasers have achieved rapid development, and the technology is becoming mature.[3–8] In the development process of this type of laser, high-quality inorganic semiconductor materials have always been the key to restricting the application of high-performance lasers. On the other hand, in the field of optical display and optical communication, due to the problems of material production and processing technology, inorganic semiconductor lasers are not easy to be integrated with all-optical panels. In comparison, organic semiconductor materials that can be used as gain media have

[a] *Department of Electrical and Electronic Engineering, Xi'an Jiaotong-Liverpool University, Suzhou, Jiangsu, 215123, P. R. China*
[b] *Institute of Functional Nano & Soft Materials (FUNSOM), Soochow University, Suzhou, Jiangsu, 215123, P. R. China. E-mail: wangxuedong@suda.edu.cn*
[c] *Oxford Suzhou Centre for Advanced Research (OSCAR), University of Oxford, 388 Ruo Shui Road, Suzhou, Jiangsu, 215123, P. R. China*
† These two authors contribute equally to this work.

Ying-Li Shi

Ying-Li Shi is a lecturer at the Department of Electrical and Electronic Engineering, Xi'an Jiaotong-Liverpool University. She received her Master's degree under the supervision of Prof. Liang-Sheng Liao and Prof. Xue-Dong Wang at the Institute of Functional Nano & Soft Materials (FUNSOM) of Soochow University in 2018. She received her PhD from the Department of Physics, The University of Hong Kong in 2022. Her research interests include organic crystals, wide bandgap metal oxide materials, and light emitting diodes.

Ling-Yi Ding

Ling-Yi Ding graduated from the University of Manchester in 2017. Her Master's degree is in Polymer Materials Science and Technology. She joined Soochow University, Institute of Functional Nano & Soft Materials (FUNSOM) in 2018. Her research focuses on spiro-based host materials.

a wide variety of sources and have the advantages of a wide and tunable emission spectrum, high photoluminescence efficiency, large absorption and emission cross-sectional area, easy film formation and processing, simple preparation of exit windows, and easy integration.[9–11] Therefore, in recent years, organic semiconductor optoelectronic devices, especially organic semiconductor lasers, have attracted more and more attention from researchers.[12–15]

Solid-state lasers consisting of organic micro-nanocrystals are expected to play a key role in novel optoelectronic devices. Thus far, self-assembled organic crystals based on various organic polymers and small molecules have been applied to realize solid-state lasers.[16–22] These organic molecules self-assemble into various ordered structures under the influence of weak intermolecular forces, such as π–π interactions, hydrogen bonds, and van der Waals forces. Compared with traditional optical gain materials (such as fluorescent dyes, semiconductor quantum dots, perovskites, small organic molecules and so on), organic micro/nanocrystals not only exhibit workable solution processability and molecular designability but also show remarkable broadband gain properties due to their multiple energy levels and excited state processes. As presented in Fig. 1, various organic lasers based on organic micro/nanocrystals have been reported with different morphologies, such as wires, tubes, fibers, rectangular disks, hexagonal

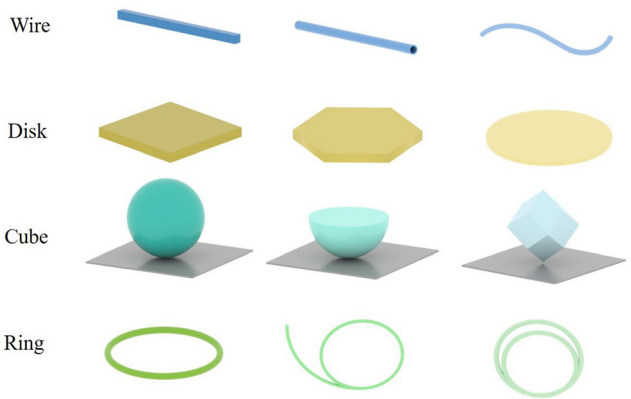

Fig. 1 Schematic illustrations of organic micro/nano-crystals with different geometries.

Yun Hu

Yun Hu is a research scientist at Oxford Suzhou Centre for Advanced Research (OSCAR), University of Oxford. He received his PhD in Physics from the Institute of Functional Nano and Soft Materials at Soochow University in 2020. His research interests include organic electroluminescent devices, organic/inorganic interfaces, and device physics.

Qiang Lv

Qiang Lv received his Master's degree from the College of Materials Science and Engineering of Beijing University of Chemical Technology in 2020. Now, he is pursuing his PhD degree under the supervision of Prof. Liang-Sheng Liao and Prof. Min Zheng at Soochow University. His current research interest is in organic low-dimensional multiblock heterostructures and their optoelectronic applications.

Wan-Ying Yang

Wan-Ying Yang received her Bachelor's degree in Pharmaceutical Engineering from the University of Taishan in 2020. Now, she is pursuing her Master's degree under the supervision of Prof. Liang-Sheng Liao and Prof. Xue-Dong Wang at the Institute of Functional Nano & Soft Materials (FUNSOM) of Soochow University. Her current research interests include the design and synthesis of organic near-infrared materials and their application in organic solid-state lasers.

Xue-Dong Wang

Xue-Dong Wang is a full professor at the Institute of Functional Nano & Soft Materials (FUNSOM), Soochow University. He received his Bachelor's degree in Chemistry at Lanzhou University in 2011 and his PhD in Physical Chemistry at the Institute of Chemistry, Chinese Academy of Sciences (ICCAS) in 2016. Dr Xue-Dong Wang's research focuses on the synthesis of organic micro/nanocrystals and organic photonics, including organic solid-state lasers and optical waveguides.

disks, circular disks, spheres, hemispheres, octahedrons, and rings (with one or two closed loops). As we summarized in previous reviews, organic crystals can be controllably prepared *via* solution process,[23,26–29] physical/chemical vapor transport,[24] and template methods,[25] wherein the solution process relying on weak interactions is the most common approach for fabricating organic crystals with unique advantages of low cost and simple operation. It is based on the self-assembly of organic molecules in the solution state to form various micro/nano-structures during the solvent evaporation process. In addition, the size, number, and position of organic crystals can be precisely controlled by the template method, and crystals with large-scale array structures can also be obtained, laying the foundation for the construction of novel multifunctional optoelectronic device arrays.[30] Furthermore, the basic parameters and emission performance of organic micro/nanocrystal based lasers, including the gain material, fabrication method, cavity morphology, resonator type, quality factor (Q), threshold, and emission wavelength are summarized in Table 1.

In this review, to emphasize the superior characteristics and summarize the achievements of organic micro/nanocrystals in the field of solid-state lasers, we herein briefly review their recent progress from the standpoint of organic molecules, morphology modulation, laser performance, and applications in high-performance organic photonic devices. Furthermore, we propose conclusions and our opinions on existing challenges and future development of organic micro/nanocrystal lasers.

2. Excited-state process for organic lasers

The realization of a laser requires three elements: excitation source, active medium, and optical resonator. Active materials play a fundamental role in lasers, which should have the following basic characteristics: (1) the material must have a suitable energy level distribution. When the material is excited, the number of particles can be reversed, which is a necessary condition for obtaining laser emission; (2) the stimulated emission cross section should be as large as possible; (3) the photoluminescence quantum yield (PLQY) of the material should be relatively high under solid-state conditions and (4) low self-absorption at laser wavelengths.[21]

Among various materials, organic molecules have abundant excited-state processes, including lots of different excited states, which can provide various inherent forms of energy level systems and are conducive to the population inversion of stimulated emission.[11,52] Many organic molecular materials have been proven to be suitable optical gain media, as shown in Fig. 2a. Typically, most organic molecules realize stimulated laser emission relying on the quasi-four-level structure formed by different vibrational energy levels of the ground state (S_0) and the first excited state (S_1). The rich excited state process of organic materials provides the possibility to construct a four-level structure that is more favorable to laser emission. As illustrated in Fig. 2b, upon excitation, the electrons transit from the lowest vibrational energy level of S_0 (E1 level) to the highest vibrational energy level of S_1 (E2 level). Then, most of

Table 1 Summary of organic micro/nanocrystal lasers with various gain materials and cavity geometries

Gain material	Fabrication method	Cavity morphology	Resonator type	Q factor	Threshold	Emission wavelength (nm)	Ref.
TPI	PVD	Wire	FP	—	—	375	20
DSB	Solution self-assembly method	Hexagonal microdisks	WGM	210	790 nJ cm^{-2}	440	31
o-MSB	Solution-drying method	Rectangular microplate	WGM	1500	540 nJ cm^{-2}	450	32
4M-DSB	Solvent diffusion method	Platelet-like crystal	FP	—	2.4 mJ cm^{-2}	465	33
DPBT	Solution-process	Wire	FP	57	60 nJ	475	34
Tpbe-Cd	Bottom-up and top-down method	Wire	FP	∼1000	522 nJ cm^{-2}	490	35
BP1T-CN	Physical vapor transport method	Rod	FP	910	178 μJ cm^{-2}	500	36
DPPDOD	Solution self-assembly method	Ring	Ring	300	—	500	37
HBT	Liquid-phase self-assembly method	Wire	FP	1500	197 nJ cm^{-2}	514	38
Dye doped PS	Emulsion-solvent-evaporation method	Circular microdisk	WGM	∼10^3–10^4	∼146 nJ	570	39
BP3T	Physical vapor transport method	Platelet	FP	—	∼370 μJ cm^{-2}	∼570	40
mp-PDI	Reprecipitation method	Hexagonal microdisk	WGM	567	10.8 μJ cm^{-2}	595	41
QD doped PVP	Direct drawing method	Ring	Ring	400	100 μJ cm^{-2}	600	16
MOF	Solution-process	Sphere	WGM	∼10^4	—	630	42
HDFMAC	Solution self-assembly method	Ring	Ring	10^3–10^4	14.2 μJ cm^{-2}	650	43
S-BF_2	Solution-process	Wire	FP	—	10.4 μJ cm^{-2}	650	44
HDMAC	Solution drop-drying method	Wire	FP	—	1.05 μJ cm^{-2}	650	45
		Rectangular microdisk	WGM	∼7000	0.43 μJ cm^{-2}		
DMHP	Bottom-up and top-down method	Wire	FP	—	1 μJ cm^{-2}	670	46
CAZ-A/CBP	Confined solution-growth method	Ring	Ring	1300	3.96 μJ cm^{-2}	683	47
DMHP	Solution-phase growth method	Wire	FP	—	1.4 μJ cm^{-2}	720	19
H2TPyP	Vaporization -condensation-recrystallization process	Rectangular microtube	FP and Ring	—	3.4 mJ cm^{-2}	730	48
DPHP	Solvent evaporation method	Hemisphere	WGM	1400	610 nJ cm^{-2}	750	49
MOF	Ion exchange	Rhombic dodecahedron	WGM	1863	17.2 μJ cm^{-2}	792	50
DDMP	Solution exchange	Nanowire	FP	2372	13.2 μJ cm^{-2}	854	51

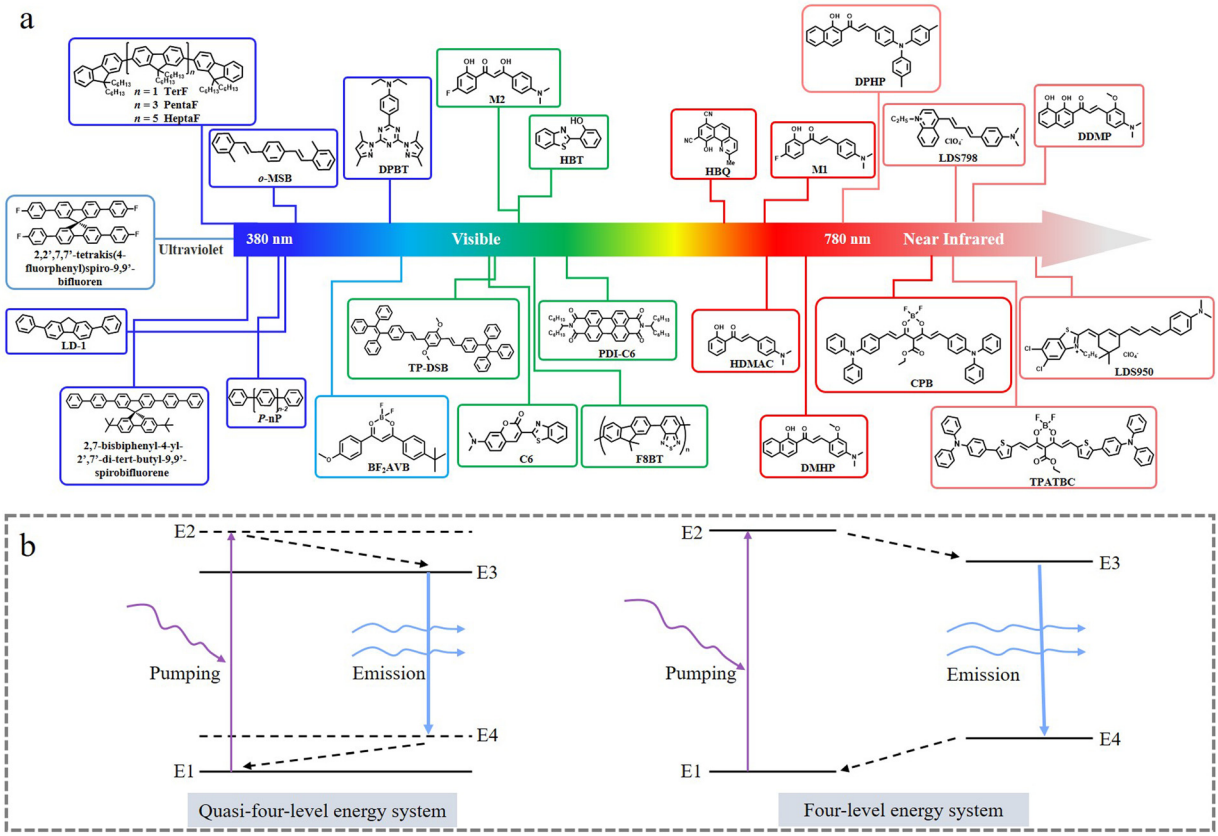

Fig. 2 (a) Molecular structures of typical organic molecular with lasing emissions from ultraviolet to near-infrared. (b) Schematic of the quasi-four-level system (left) and four-level system (right).

the excited state electrons will undergo fast relaxation to lower vibrational level S_1 (E3 level). Excited state electrons at the E3 level transition vertically to the high vibrational energy level (E4 level) of S_0 and then reach the E1 level through vibrational relaxation. Due to the extremely short decay time of the vibrational relaxation, the accumulation of electrons at the E4 level can be effectively blocked. Therefore, the number of electrons in the E3 level is always more than that in the E4 level, which is prone to population inversion and stimulated emission.[1]

3. Aggregation mode and crystal morphology

Compared with inorganic materials composed of strong chemical bonds, organic materials are supported by weaker intermolecular forces, so it has been confirmed that the morphology of micro/nanocrystals can be modulated by adjusting the intermolecular forces to affect the molecular packing mode.[53] For example, Prof. Yao and co-workers prepared organic crystals of naphthalene derivatives with different geometries: nanowires and nanosheets by controlling the main intermolecular interactions (including H bonding and π–π stacking) through the reasonable molecular design (Fig. 3a).[54] In our work, we investigated the side-chain effect on organic crystals. The organic molecules with different side chains were designed to modulate the intermolecular interaction, including 1,4-bis(2-methylstyryl)benzene (*o*-MSB),1,4-bis(3-methylstyryl)-benzene (*m*-MSB) and 1,4-bis(4-methylstyryl)benzene (*p*-MSB). As shown in Fig. 3b, the shapes of *o*-MSB, *m*-MSB, and *p*-MSB microsheets are rectangle, parallelogram, and hexagon, respectively, with the corresponding inner angles of 90°, 80°, and 103°.[32,55] In addition, it has been reported that the solubility of organic molecules, the choice of different solvents, the assistance of surfactant or template, *etc.*, can affect the crystal nucleation process and then result in different morphologies of the organic micro/nanostructures.[46,53,56–59] For example, Prof. Huang and co-workers constructed three microstructures of 9,9′-(2,5-dibromo-1,4-phenylene)bis(9*H*-carbazole) (PDBCz) microsheets *via* altering the solution concentration (Fig. 3c).[60] It has been proved that the concentration-dependent polymorphs are ascribed to the supersaturation-controlled kinetic nucleation and crystallization process. Combined with the simulation results, they deduced that π–π interactions are the dominant driving force during the growth of rhomboid microsheets at low solution concentrations. In contrast, at high concentrations, π–π stacking and halogen–π interactions are the direct driving force for the formation of rectangular and hexagonal microsheets. In overall, it is still a challenge in the accuracy control of the morphology with a defined shape and desired performance for organic micro/nanocrystals.

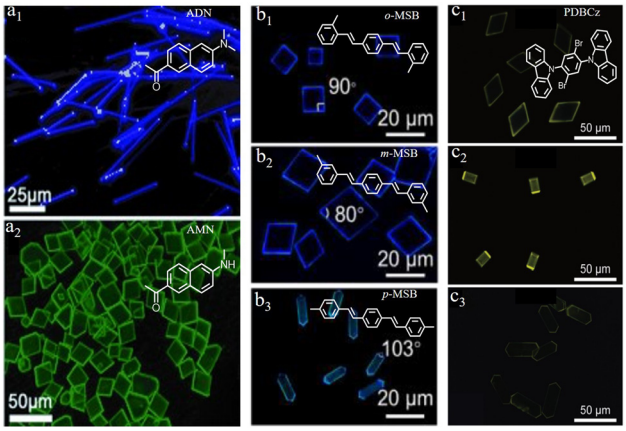

Fig. 3 Tunable microstructures of organic crystals. (a) The PL microscopy images of 1D and 2D nanostructures based on naphthalene derivatives with different amino groups.[54] Copyright 2013 Wiley-VCH Verlag GmbH & Co. KGaA, Weinheim. (b) The PL microscopy images of *o*-MSB, *m*-MSB, and *p*-MSB microsheets with different side chains.[55] Copyright 2022 Elsevier. (c) The PL microscopy images of concentration dependent PDBCz microsheets. Insets are the corresponding molecular formulas.[60] Copyright 2021 The Royal Society of Chemistry.

4. Organic lasers

Organic semiconductor molecules are ideal candidates for organic solid-state lasers due to their large absorption and radiation cross-sections, inherent quasi-four-level systems, abundant molecular structures, and solution processability. In particular, organic micro/nanoscale crystals self-assembled through weak non-bonding interactions (including π–π interactions, hydrogen bonds, halogen bonds, and van der Waals interactions) between organic molecules can serve as gain media and resonate simultaneously. Therefore, it presents a good application prospect in organic solid-state lasers. Since Tessler *et al.* first reported the vertical microcavity laser based on organic conjugated polymer material, poly(*p*-phenylenevinylene), in 1996, many researchers have carried out a lot of research on organic semiconductor materials and the design of various resonator structures and have achieved certain results.[61] Typical optical cavities include planar Fabry–Perot (FP) cavity,[20,62] distributed feedback (DFB) resonator,[21,63,64] random cavity,[65,66] chaotic cavity,[67] ring resonator,[16,37,68] whispering gallery mode (WGM) cavity[30,69] and photonic crystal lasers.[70,71] In this section, we will introduce some representative works on organic lasers with different structures and cavities.

4.1 Organic lasers with Fabry–Perot cavities

One-dimensional (1D) crystals, including structures such as wires, tubes, fibers, *etc.*, have drawn much attention over the past few decades as a result of their inherent two-dimensional quantum confinement effect, which makes them promising in applications for basic units in optoelectronic devices such as electrochemical sensors, light-emitting diodes, field-effect transistors, solar cells and so on. 1D crystals with flat end facets and effective optical confinement can serve as Fabry–Pérot (FP) cavities for organic lasers. As illustrated in Fig. 4a, the FP cavity

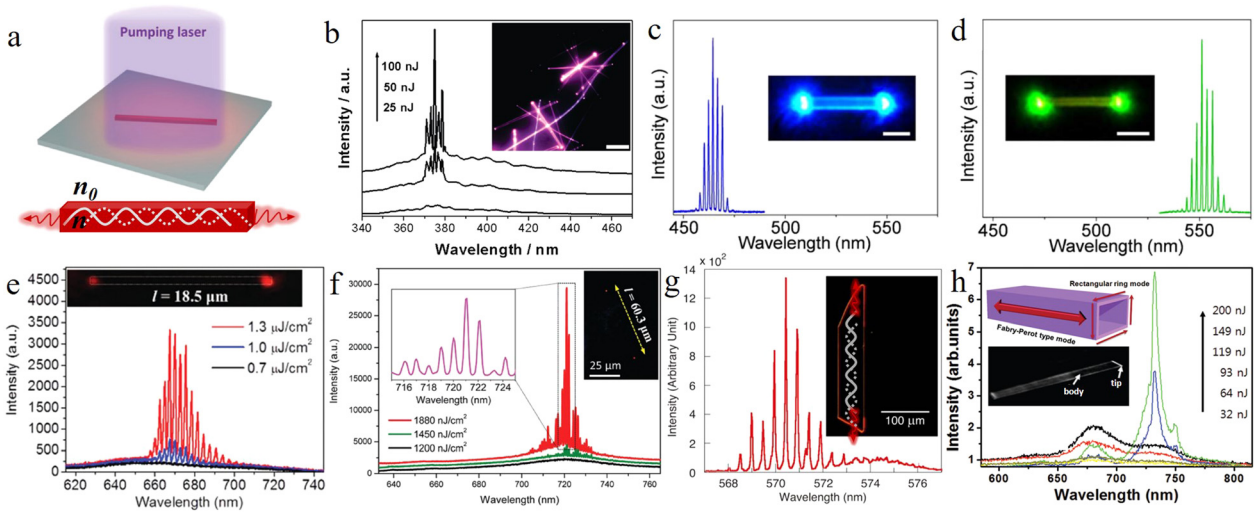

Fig. 4 Organic crystal lasers with color tunability and FP resonator. (a) Up: the schematic diagram of a single nanowire pumped by laser. Bottom: An organic nanowire functions as the optical waveguide.[19] Copyright 2017 Wiley-VCH Verlag GmbH & Co. KGaA, Weinheim. (b) The PL spectra of the TPI wire with the pump energy increasing from 25 to 100 nJ. Inset: The PL microscopy image of TPI nanowires.[20] Copyright 2008 Wiley-VCH Verlag GmbH & Co. KGaA, Weinheim. (c and d) Lasing spectra of OPV-A and OPV-B nanowires pumped with 400 nm laser, respectively. Insets are the corresponding PL images of the OPV-A and OPV-B nanowires.[72] Copyright 2017 Science. (e) The PL spectra of DMHP nanowire under different excitation energies. Up inset: PL microscopy image of one DMHP nanowire with a length of 18.5 μm.[46] Copyright 2018 The Royal Society of Chemistry. (f) The PL spectra of DMHP nanowire excited at different energies (1200 to 1880 nJ cm^{-2}). Left inset: magnified spectrum at around 720 nm. Right inset: the PL microscopy image of DMHP nanowire with a length of 60.3 μm.[19] Copyright 2017 Wiley-VCH Verlag GmbH & Co. KGaA, Weinheim. (g) The PL spectra of BP3T crystal platelet with sharp and parallel crystal edges. Inset: The PL microscopy image of BP3T crystal.[40] Copyright 2012, Nature Publishing Group. (h) PL spectra of the H_2TPyP-RMT tube. Up insert: Schematic diagram of the resonator modes in the H_2TPyP-RMT. Bottom insert: the PL microscopy image of H_2TPyP-RMT tube.[48] Copyright 2011, American Chemical Society.

or FP interferometer is one of the most fundamental and ordinary building blocks of laser interferometers, which contains two mirrors facing each other, and the active material is sandwiched with the mirrors.[19] Under the relationship of $2nL/\lambda = m$, wherein n is the refractive index of the active material and m is an integer, single-mode or multi-mode laser can output.

In 2008, Prof. Yao and co-workers confirmed the feasibility of achieving the optically pumped laser behavior in small organic molecules.[20,62] They prepared the single crystalline nanowires of 2,4,5-triphenylimidazole (TPI, Fig. 4b) using the adsorbent-assisted physical vapor deposition (PVD) approach. The TPI wires exhibit a purple to ultraviolet emission from the PL microscopy image. When increasing the pump energy from 25 to 100 nJ, amplified spontaneous emission with a wavelength at around 375 nm is observed. At lower pump energy (below threshold), the PL intensity increases almost linearly with the excitation density. When increasing to the critical value, the gain increases substantially. As organic semiconductor lasers develop, the laser emission peak can be regulated from ultraviolet to near-infrared. For example, Prof. Zhao and co-workers selected two organic laser dyes (cyano-substituted oligo(*p*-phenylenevinylene), OPV-A and cyano-substituted oligo-(*a*-phenylenevinylene)-1,4-bis(*R*-cyano-4-diphenylaminostyryl)-2,5-diphenylbenzene, OPV-B) with high optical gain properties, and fabricated regularly shaped organic single crystal nanowires of these two dyes through controllable self-assembly method.[72] As shown in Fig. 4c–d, multimode laser actions with the emission peaks at ~464 and ~555 nm are observed in the OPV-A and OPV-B nanowires, respectively. As can be seen from the inset PL images, the OPV-A and OPV-B nanowires excited above the lasing threshold exhibit two impressive luminescent spots on both the end faces along the length of the nanowire, which is a typical characteristic of FP mode optical resonators.

In 2018, our group reported a collaborative approach of bottom-up/top-down processes to prepare uniform nanowires based on (*E*)-3-(4-(dimethylamino)-2-methoxyphenyl)-1-(1-hydroxynaphthalen-2-yl)prop-2-en-1-one (DMHP) with a diameter around 120 nm, wherein the bottom-up method depends on chemical or physical interactions to assemble individual units into highly ordered structures and unique hierarchical microstructures (Fig. 4e).[46] This obtained DMMP nanowire shows strong red laser emission (λ = 670 nm) when the excitation energy exceeds the threshold of 1.0 mJ cm^{-2}. At present, near-infrared (NIR) laser has great application potential in the fields of environmental monitoring, laser communication, and medical treatment. However, it is relatively more difficult to realize than that of the organic lasers with other colors because of the low emission efficiency of near-infrared organic materials.[49] Recently, our group reported a tunable NIR laser based on the self-assembled organic nanowire with a laser peak at 720 nm.[19] The PL spectrum under different pump energies of single *(E)*-3-(4-(dimethylamino)2-methoxyphenyl)-1-(1-hydroxynaphthalen-2-yl)prop-2-en-1-one (DMHP) nanowires with the length of 60.3 μm is exhibited in Fig. 4f. Impressively, these DMHP nanowires' FP cavity can achieve single (660 or 720 nm) and dual-wavelength (660 and 720 nm) laser action due to the intrinsic self-absorption by adjusting the length of nanowires, which confirms the length-dependent modulating effect and intrinsic lasing properties in 1D organic crystals.[10,73]

In irregular disk-shaped organic crystals, Taishi Takenobu and co-workers reported FP-type resonators.[40] They chose single crystals of α,ω-bis(biphenyl)terthiophene (BP3T) as the active material for resonators prepared *via* the physical vapor transport method (Fig. 4g). It was found that the BP3T crystal with narrow width and naturally-formed parallel crystal edges can act as an FP optical resonator. The laser oscillation spectrum of BP3T single crystal is obtained with the emission peak at ~570 nm. The inset presents the optical micrograph image of an individual BP3T crystal under excitation with shiny non-parallel edges. In addition, Yoon *et al.* first observed the lasing behavior in rectangular microtubes with sharp bend over at 90 degrees and nanoscale wall thicknesses *via* the vaporization condensation-recrystallization approach. There are two types of cavity modes in this microtube: one is that the FP mode resonates along the growth direction of the tube, and another is that the ring mode resonates by waveguiding alongside the rectangular bending corners (Fig. 4h). As the pump energy is above the threshold of 3.4 mJ cm^{-2} (119 nJ), laser behaviour in tetra(4-pyridyl)-porphyrin (H_2TPyP) microtubes is observed.[48]

4.2 Organic whispering-gallery-mode lasers

Among different modes of resonators, whispering gallery mode (WGM) resonators are the most popular ones and have been proven to be excellent candidates for the fabrication of low threshold and narrow linewidth lasers due to their low optical loss and miniature sizes, such as high Q and small mode volume (V).[23,69] Since Garrett and co-workers first realized the WGM laser of spherical CaF_2:Sm^{2+} in 1961, various materials have been investigated to construct WGM lasers, such as inorganic and organic semiconductors.[74] In our work, we firstly achieved the WGM laser in hexagonal microdisks of *p*-distyrylbenzene (DSB) (Fig. 5a) using the solution self-assembly approach.[31] In hexagonal microdisks, 6-WGM, 3-WGM or D3-WGM cavities can be formed depending on how light is reflected, wherein the 6-WGM is the most common one wherein the light is reflected by the six lateral sides. For example, Prof. Fu and co-workers reported the laser action in 6-WGM microcavity of *N*,*N*′-bis(1-ethylpropyl)2,5,8,11-tetrakis(p-methyl-phenyl)-perylene-diimide (mp-PDI) based hexagonal microdisks.[41] Prof. Zhao and co-workers simultaneously achieved dual-wavelength lasing action with peaks at 527 and 562 nm, respectively, in hexagonal microdisk constituting the 6-WGM type resonator.[75] However, in our work, based on the following two phenomena/reasons, we concluded that the DSB based microdisks function as the D3-WGM cavity. Firstly, the inset PL image of Fig. 5b shows the alternating bright/dark sides of the individual DSB microdisks under excitation, which is consistent with the properties of 3-WGM or D3-WGM microcavity, *i.e.*, the cavity consists of three lateral sides. Secondly, the fitting results of group refractive index based on 3-WGM and D3-WGM in hexagonal microdisks with different sizes confirmed that D3-WGM is the feedback mode of our samples. The PL spectra under different pump densities, increasing from 300 to 1170 nJ cm^{-2}, indicate the laser action with sharp

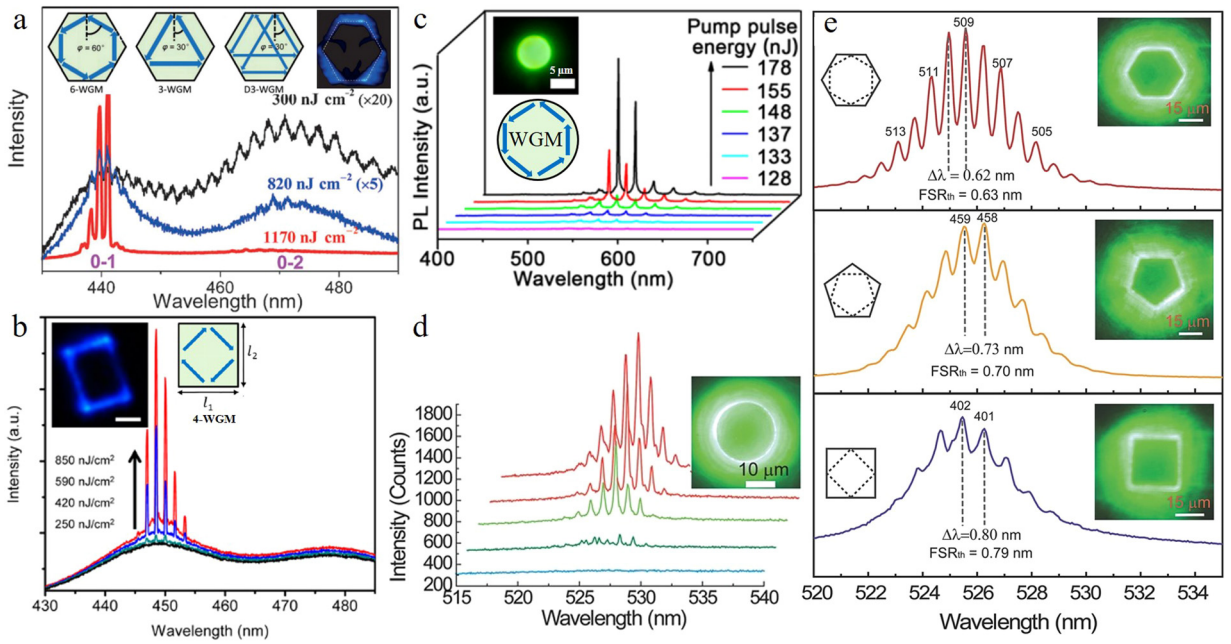

Fig. 5 WGM laser performance of organic micro/nanocrystals. (a) The PL spectra of DSB hexagonal microdisk with an edge length of 2.7 mm. Inserts are schematic images of the light-path of 6-WGMs, 3-WGMs, D3-WGM and the PL microscopy image of DSB microdisk, respectively.[31] Copyright 2014 Wiley-VCH Verlag GmbH & Co. KGaA, Weinheim. (b) The PL spectra of *o*-MSB rectangular microplate pumped with different laser energies (250, 420, 590, and 850 nJ cm^{-2}). Inserts are the PL microscopy image of o-MSB microplate and the schematic figure of the light-path of 4-WGM in the rectangular crystal.[32] Copyright 2014, American Chemical Society. (c) The PL spectra of dye-doped PS microdisk. Inserts are the corresponding PL microscopy image and light-path in the microdisk.[39] Copyright 2015, American Chemical Society. (d and e) The PL spectra of BP2T circle, hexagonal, pentagonal, and square microdisks. Inserts are the corresponding PL images of these microdisks.[30] Copyright 2013 Wiley-VCH Verlag GmbH & Co. KGaA, Weinheim.

peaks (~440 nm) on the top of the 0–1 transition. In addition, we prepared rectangular microplates of 1,4-bis(2-methylstyryl)-benzene (*o*-MSB) *via* a solution-drying method.[32] The as-prepared *o*-MSB rectangular microplates are with regular shapes and good light-confinement ability. Therefore, lasing action is observed in these rectangular microplates with an emission peak at 450 nm, high Q of ~1500, and low threshold of ~540 nJ cm^{-2}. The corresponding cavity mode is 4-WGM (right inset of Fig. 5b) because the light is totally reflected on the four sides of the *o*-MSB rectangular microplate (left inset of Fig. 5b). We also prepared 3-[4-(dimethylamino)phenyl]-1-(2-hy-droxyphenyl)prop-2-en-1-on (HDMAC) rectangular microdisks, which provide the 4-WGM resonator for lasing oscillator with Q as high as ~7000.[45]

Compared with cavities discussed above, the inherent properties of circular microdisks, such as ultra-smooth surfaces and perfectly circular boundaries, can supply adequate feedback for realizing high-performance laser oscillation. Herein, Prof. Zhao and co-workers proposed an emulsion-solvent-evaporation strategy to produce flexible and circular microdisk WGM resonators based on polystyrene (PS) doping with organic dyes (Fig. 5c).[39] As shown in the insert PL image of the circular microdisk, under pump excitation, intense emission was observed along their circular boundaries, which is the typical characteristic of the WGM cavity. The diameter of the circular microdisk can be controlled from 4 to 20 μm by changing the micelle size of the emulsion during the preparation process. Meantime, the lasing properties of these flexible WGM resonators, including the mode spacing and *Q* factor, were also well-changed with the diameter of the microdisks. The researchers found that the bending radiation loss of a circular resonator declines exponentially with its size, so the *Q* factor increases with the increase in the diameter. Using the combination of photolithography and reactive-ion etching method, Prof. Sun and co-workers fabricated WGM microcavity arrays and observed lasing oscillations from circular, hexagonal, pentagonal, and square microdisks, respectively (Fig. 5d and e).[30] This strategy for producing large-area crystal arrays is applicable for 2,5-bis(4-biphenylyl)thiophene (BP1T) and 2,5-bis(4-biphenylyl)bithiophene (BP2T) crystals, which is essential for future development of organic crystal lasers as functional components in integrated photonics applications.

With the continued development of organic crystals, researchers discovered that hemispherical and spherical microcrystals are applicable as WGM resonators in organic lasers. For example, we successfully synthesized (*E*)-3-(4-(di-ptolylamino)-phenyl)-1-(1-hydroxynaphthalen-2-yl)prop-2-en-1-one (DPHP) micro-hemispheres with NIR laser emission. The DPHP hemisphere based WGM cavity has a high *Q* of 1400 and low threshold of 610 nJ cm^{-2} (Fig. 6a). Following this work, we obtained (*E*)-3-(4-(dip-tolylamino)phenyl)-1-(4-fluoro-2-hydroxyphenyl)prop-2-en-1-one (DTPHP) microspheres with different diameters, which can also serve as WGM resonators.[76] In 2017, Yohei Yamamoto and co-workers chose the miniemulsion method to prepare microspheres using different polymer materials with blue to red colors and reported WGM lasing of these microspheres.[18] Prof. Zhao and co-workers reported a series of research results in the

preparation of spherical organic crystals. For example, they first obtained microspherical cap-shaped organic crystals with red-green-blue (RGB) laser emission based on WGM resonators through the inkjet printing method.[77] Immediately afterward, they realized tunable polychrome single-mode lasers in heterogeneously coupled WGM microresonators consisting of different spherical microcavities. Due to the high flexibility and compatibility of organic materials, the emission wavelength of single-mode lasers can be freely tuned by adjusting the optical gain in the coupled cavity.[78] As presented in Fig. 6b, they also reported an approach to prepare binary organic microspheres, which can function as WGM cavities in dual-color lasers.[79] In this method, two polymer matrix materials with different polarities, polystyrene (PS) and poly(methyl methacrylate) (PMMA), were used to form the Janus laser. Organic dyes, 1,4-bis(α-cyano-4-diphenylaminostyryl)-2,5-diphenylbenzene (CNDPASDB, hydrophobic) and rhodamine-101 (Rh101, hydrophilic), with different color and polarity, were chosen as the active gain. The parallel-aligned hemispheres in the Janus structure are formed with two independent WGM cavities, which makes the color-tunable by changing the excitation position. Under excitation, three separate sets of dual-color laser emissions are obtained with violet-blue, cyan-red, and green-orange, respectively. Subsequently, they reported an approach to obtain wavelength tunable spherical microcrystals based on an organic dye doped polymer. The WGM organic resonators can modulate the lasing wavelengths by changing the dye doping ratio.[80] In 2021, they successfully constructed metal–organic frameworks (MOFs) microspheres with a high Q factor reaching 10^4, which can provide sufficient feedback for the laser oscillation.[42] In addition, they also developed metal-organic framework organic crystals with rhombic dodecahedron structure (Fig. 6c). In this work, the organic NIR dye, 4-[4-[4-(dimethylamino)phenyl]-1,3butadienyl]-1-ethyl quinolinium perchlorate (LDS 798), was used as the gain medium. Rho-ZMOF $[In_{48}(C_5N_2O_4H_2)_{96}\cdot(C_7N_3H_{15})_{24}]$, was the host matrix to encapsulate LDS 798 *via* the ion-exchange process. According to the simulated field intensity distribution result (right insert in Fig. 6c), it was verified that the six facets marked in red could provide sufficient optical confinement as reflectors. The PL image of LDS 798@*rho*-ZMOF microcrystals (left inset in Fig. 6c) also confirmed that the bright laser emission is mainly output from the six facets of the crystal, which is typical for the WGM cavity. Pumping above the lasing threshold, NIR microlasers is realized with a low threshold of ~17.2 μJ cm^{-2} and a large Q of 1863. A series of progress achieved by Prof. Zhao's research group provides theoretical and experimental strategies for realizing of full-color laser displays with excellent color expression.

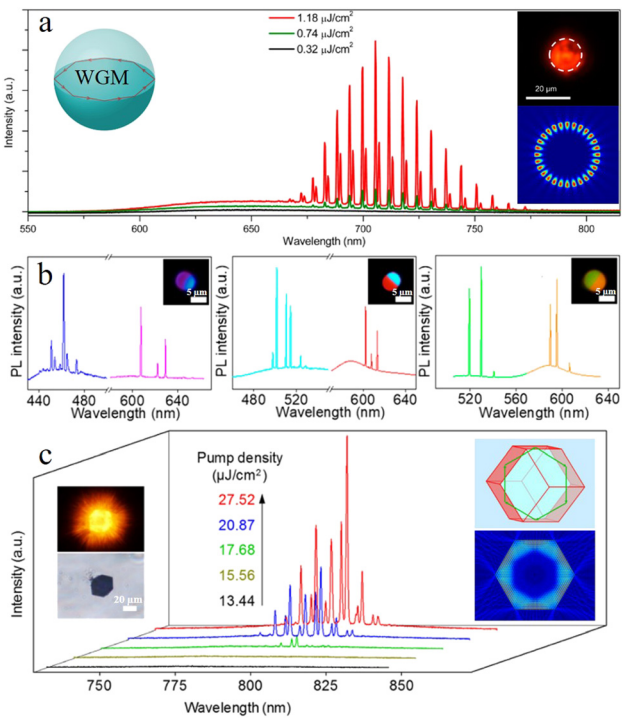

Fig. 6 (a) The PL spectra of single DPHP hemispherical crystal with a diameter of 14.4 μm. Right inset: the magnified spectrum around 760 nm. Right insets are the PL microscopy image of the corresponding hemisphere and the simulated electric field distribution in the hemispherical crystal. Left inset describes the light propagation in the hemisphere resonator.[49] Copyright 2015, American Chemical Society. (b) The PL spectra of Janus microspheres doped with different organic dyes. Inserts are the corresponding PL microscopy images.[79] Copyright 2019, American Chemical Society. (c) The PL spectra of the LDS 798@rho-ZMOF rhombic dodecahedron microcrystal under different pump energies. Left inserts are the bright-field microscopy image and PL microscopy image of the crystal. Right inserts are the simulated crystal morphology of the crystal and the simulated field intensity distribution in the crystal.[50] Copyright 2018, American Chemical Society.

4.3 Organic lasers with ring resonators

Ring resonator with a circular structure or closed loop structure is another option for achieving laser action, in which light can be excellently confined by the total internal reflection on the curved outer surface. However, the construction of ring resonators is still challenging because of their low structural quality of optical defects or a tiny size below diffraction limits.[37,81] Prof. Fu and co-workers constructed microring resonator arrays with controllable size distribution and uniform geometry by a restricted solution-growth method.[47] In their research, the carbozyl borondifluoride curcuminoid derivative (CAZ-A) was mixed into a host material of 4,4′-bis(*N*-carbazolyl)-1,10-biphenyl (CBP). By changing the doping ratio of CAZ-A, the laser emission can be adjusted from 650 to 725 nm. The CAZ-A/CBP crystal arrays serve as ring resonators and present excellent laser performance with a Q factor of ~1300 constitute resonators. As shown in Fig. 7a, when the individual microring is pumped with different excitation energy, the μ-PL spectra present the multimode laser emission with a group of sharp peaks in the 670–705 nm range above the threshold. The corresponding PL image (inset of Fig. 7a) obviously presents a waveguide along the ring. Prof. B. J. Li and co-workers fabricated ring nanowires using the CdSe–ZnS quantum dot (QD) doped polyvinylpyrrolidone (PVP) and formed the ring resonator-based multimode laser emission with the Q factor of 400 and threshold of 100 μJ cm^{-2}.[16] It is found that the size (such as the large and small diameter) and shape of the ring can affect the laser properties of the ring resonator.

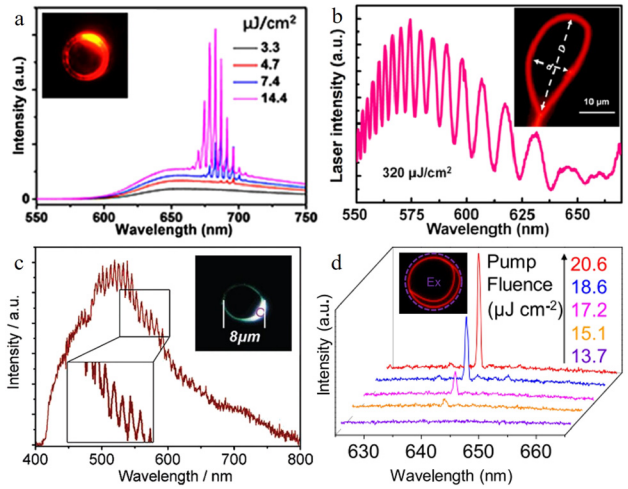

Fig. 7 Laser performance from ring resonators of organic micro/nanocrystals. (a) The PL spectra of CAZ-A/CBP microrings at different pump energies with a diameter of 19 μm. Insert is the PL microscopy image of this corresponding microring excited above the laser threshold.[47] Copyright 2019, American Chemical Society. (b) The PL spectrum of QD doped PVP ring nanowire pumped with the density 320 μJ cm^{-2}. Inset: PL microscopy image of an individual ring with D is 26 μm and d is 11 μm.[16] Copyright 2014, American Chemical Society. (c) The PL spectrum of single DPPDO microring with a diameter of 8 μm. The excitation position is marked with a violet circle. Inset is the PL microscopy image of the corresponding microring pumped with the focused 351 nm laser.[37] Copyright 2013 Wiley-VCH Verlag GmbH & Co. KGaA, Weinheim. (d) The PL spectra of the HDFMAC double-microring as a function of pump density. Insert is the PL microscopy image of a coupled ring resonator.[43] Copyright 2019, American Chemical Society.

For example, they found that the *Q* factor, the mode number, and the laser emission spectrum can be tuned *via* the refined micromanipulation of the ring resonator. Their results provide an option for the controllable multimode laser emission *via* the appropriate construction of the ring resonator. Fig. 7b is the PL microscope image and corresponding PL spectra of an individual QD-doped polymer ring with a circumference of 70 μm, which is pumped at one end with a pump density of 320 μJ cm^{-2}. The multimode resonance laser emission occurred in the region from 550 to 650 nm. Prof. Y. S. Zhao and co-workers reported the growth of 1,5-diphenyl-1,4-pentadien-3-one (DPPDO) microrings *via* a self-assembly method.[37] In the preparation process, the geometry of the microcrystal can be tuned from wire to rings and then to titles by adjusting the solution concentration driven by the interfacial tension of the solution. The self-assembled DPPDO microrings can guide and confine the optical signals efficiently and function as the ring resonator. As shown in Fig. 7c, when the individual mircoring is pumped, the light is waveguided and observed from the entire rings with strong laser emission with a peak at 500 nm. Based on this work, they prepared 3-[4-(dimethylamino)phenyl]-1-(2-hydroxy4-fluorophenyl)-2-propen-1-one (HDFMAC) microbelt-coupled microrings and double microrings by changing the ratio of two solvents (dichloromethane and ethanol), respectively (Fig. 7d).[43] The *Q* factor of microbelt-coupled microring is on the order of 10^3 to 10^4 with low threshold of ~14.2 μJ cm^{-2}. In the first step, as the solvent evaporates, HDFMAC grows in one dimension. Since dichloromethane evaporates faster than ethanol, the remaining solution on the substrate is mainly composed of ethanol, which gradually forms quasi-hemispherical droplets and serves as a circular template for the ring structure. Next, as the solvent evaporates, driven by the surface tension, the crystal grows into a curved belt encircling the droplet, eventually forming the microrings. As presented in Fig. 7d, when the double-structured ring was excited uniformly, the bright red emission along the border indicates efficient optical coupling between the two rings. The corresponding PL spectra represent the single-mode lasing emission.

5. Organic laser arrays

The earliest organic lasers can be traced back to the research on organic dye lasers in 1964, and now the research on organic semiconductor lasers has begun, and many breakthroughs have been made in the past few decades. With the further development of social science and technology, the application of organic lasers in many fields of scientific research and social life will be increasingly extensive.[17,82–84] Organic crystal laser has great flexibility in the selection of laser materials due to its rich molecular types, designable molecular structure, and adjustable performance. In particular, the preparation of directional and precisely controlled organic semiconductor single crystal arrays is of great significance for the further development of high-performance optoelectronic devices and integrated circuits. Organic semiconductor crystals have the advantages of inherent long-range order, no grain boundaries, and low defect density. Uniformly oriented single crystal arrays are beneficial to reduce integration crosstalk and performance variance in devices. However, the nucleation and growth process of organic semiconductor crystals is complex, and it is still challenging to achieve the patterned preparation of organic semiconductor single crystal arrays with uniform orientation. In the past few years, many researchers have devoted themselves to studying how to fabricate organic crystal arrays efficiently and controllably and have obtained several feasible fabrication techniques, such as inkjet printing, photolithography, and rapid evaporation.[30,47,77,85–87] In this section, we will present representative works of organic micro/nanocrystal laser arrays and their applications.

5.1 High-security cryptography

Encryption is an essential part of modern life, allowing sensitive information to be shared securely. In traditional encryption, the sender and receiver of a particular message determine a cipher or key, so only those who know the key can decrypt the message. But as computers got faster and more powerful, encryption codes became easier to break. Laser technology holds promise for ultra-fast and ultra-secure encryption. For example, Pappu *et al.* used speckle patterns generated by multiple scattering of laser light in heterogeneous media to construct high-safety optical physical unclonable functions

(PUFs) for the first time.[88–90] Organic microcrystal lasers integrate high-quality optical resonators and efficient gain media in a single architecture for efficient and large-scale patterning without complex electronic circuit fabrication and have great prospects in high-security cryptography applications. In our work, we utilized 'capillary-bridge lithography' technique and fabricated organic laser arrays employing (*E*)-3-(4-(dimethyamino)2-methoxyphenyl)-1-(1-hydroxynaphthalen-2-yl)prop-2-en-1-1 (DMHP) molecular (Fig. 8a and b).[86,87,91] During the evaporation of organic solvents, two situations occur: symmetric breakup of the liquid gives rise to discrete capillary bridges with nearly equal liquid volumes (Fig. 8a); (ii) asymmetric liquid breakup is with distinct differences in capillary bridge volumes (Fig. 8b). Capillary bridges of the same volume can produce crystals of the same length. Different capillary bridge volumes produce unequal amounts of organic molecules, resulting in organic crystals with random lengths. Therefore, the randomness of the organic crystal array can be effectively controlled by using solvents with different boiling points, including dichloromethane (DCM), 1,3-dichloropropane (DCP), 1,2- dichloroethane (DCE), and 1,4-dichlorobutane (DCB) (Fig. 8c). We find that the laser emission wavelength is strongly dependent on the length of the nanowire: lasing at 660 nm occurs in a cavity of 10 μm, lasing at both 660 nm and 720 nm in a cavity length of 30 μm, but only 720 nm occurs as cavity length increases to 70 μm. As presented in Fig. 8d, we explored the cryptographic realization of this dual lasing emission system by collecting lasing spectra on large-scale and random-sized arrays. Combined with the custom-written code, four types of laser emissions are identified through the automatic judgment of emission spectra, namely, no laser (spontaneous emission), 660 nm, 660 and 720 nm, and 720 nm lasers. Compared to conventional organic lasers, where the difference in peak number/spacing is subtler, the dual laser emission of the DMHP wires provides more reliable and stable characteristics for efficient authentication of code bits. Fig. 8e is the schematic diagram of authentication of photonic cryptographic primitives. Randomly sized arrays were excited by the pump laser, and we identified the lasing mode and encode them as cryptographic bit sequences. The 64 × 16 random quaternions were separated by these four types of laser emission (Fig. 8g). A 64-bit quaternary key provides a theoretical key space size 19 orders of magnitude larger than that of the 64-bit binary key. To convert the quaternary key into a binary key, we set the coding rules: "00" means no laser, "10" means 660 nm laser, "01" means 720 nm laser, "11" means 660 and 720 nm laser (Fig. 8h). Statistics of hamming distances for quaternary and double-binary keys are illustrated in Fig. 8f, respectively. The distribution results indicate that at least 50% and 30% of bits in each two quaternary and double-binary keys differ, respectively. Our results confirm the application of organic crystal laser arrays with highly reliable and stable dual-laser behavior in high-security encryption.

5.2 Display

With the continuous development of information technology, the new media age has come, showing that as the most vital information output terminal in the human–computer information interaction link, it has pervaded all aspects of people's lives. In today's era, display technologies emerge in an endless stream, all of which aim to achieve ultra-high-resolution, large-size, and extreme true-color displays to meet people's needs for the ultimate in beautiful vision. The goal is to achieve high-fidelity image reproduction. Laser display is a new display technology that uses lasers with three primary colors as the display light source. The laser spectrum is very narrow, called the line spectrum, with high color saturation, which can better reflect the true color of nature and form a large color gamut space on the chromaticity diagram.[92–95] Laser display technology is becoming the mainstream technology of the next-generation display industry.[96] Optically pumped

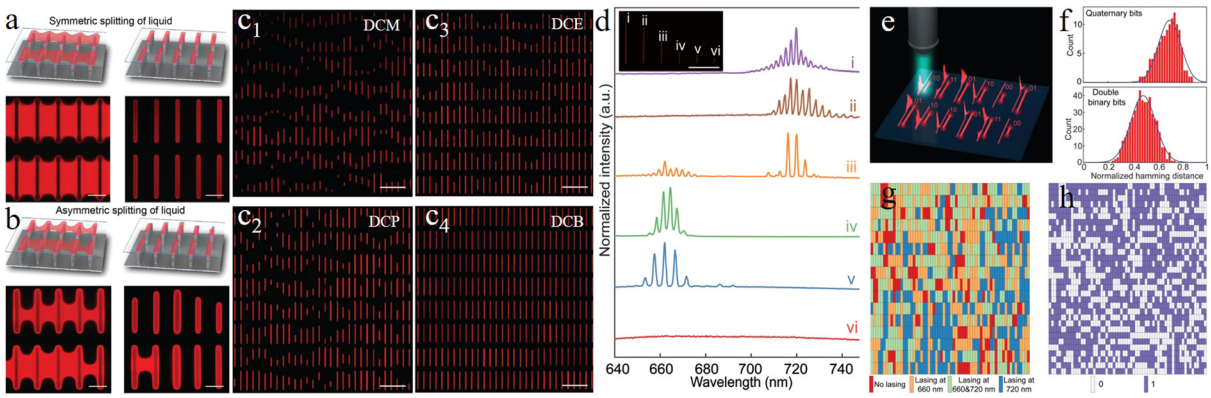

Fig. 8 Fabrication process and application of DMHP organic laser arrays. (a and b) The schematic diagram (top) and corresponding PL microscopy image (bottom) of the capillary-bridge assembly system using different solvents representing symmetric (a) and asymmetric (b) splitting of liquid, respectively. (c) PL microscopy images of nanowire arrays prepared *via* four solvents: DCM (c_1), DCP (c_2), DCE (c_3), and DCB (c_4). Lasing emission on random size nanolaser arrays. (d) The PL spectra of a random-sized nanowire sequence. Inset is the corresponding PL microscopy image of organic nanowires with different sizes. (e) The schematic diagram of authentication of photonic cryptographic primitives. The organic array is pumped with a focused laser beam to detect the laser emissions and encode them as cryptographic bit sequences. (f) The distribution of normalized Hamming distance measured for 1024 quaternary-bit keys (up) and 2048 binary-bit keys (bottom). (g) The 64 × 16 quaternary random bits. (h) The 64 × 32 double binary bits.[87] Copyright 2019 Wiley-VCH Verlag GmbH & Co. KGaA, Weinheim.

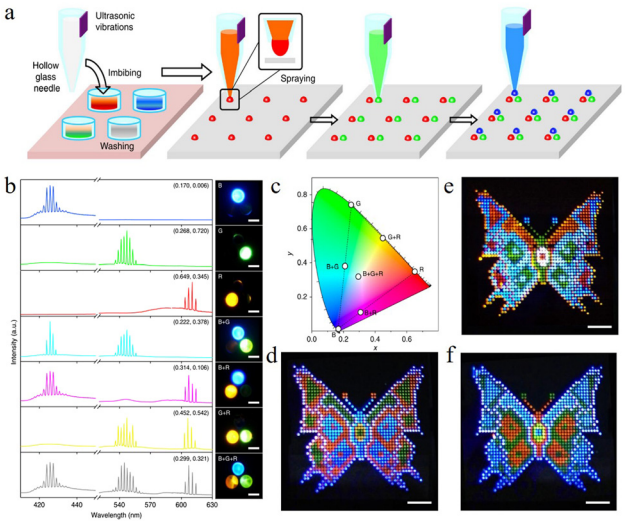

Fig. 9 Construction and application of organic microlaser arrays using an ultrasonic vibration-assisted inkjet printing method. (a) Schematic representation of the fabrication process of organic pixel arrays. (b) Full-colored and tunable laser spectra of the organic RGB spherical caps. Right are the corresponding PL microscopy images excited above their thresholds. From top to bottom are the blue (B), green (G), red (R), blue and green (B + G), blue and red (B + R), green and red (G + R), and blue, green and red (B + G + R) spherical caps. (c) Chromaticity of the laser emission peaks extracted from the PL spectra in Figure b, marked with seven white circles. The dashed lines represent the range of the obtained color gamut for the RGB pixel. (d–f) Effect images of laser display prototypes (44 × 44 pixel) with different color distributions using a similar full-color panel.[77] Copyright 2019, Nature Publishing Group.

semiconductor laser, especially the organic material, is said to deliver high optical power with good beam quality. As introduced in section 4.2, Prof. Zhao's group has made a series of achievements in the direction of organic crystal laser-based display.[77–80,92,94] As shown in the schematic diagram in Fig. 9a, the fabrication of organic RGB microlaser pixel arrays is through printing organic ink solution droplets at specific positions on substrates in line with the predesigned digital patterns with the help of ultrasonic.[77] The lasing wavelength for individual pixels can be tuned by incorporating different organic dyes into the ink solution, wherein rhodamine B (RhB), fluorescein disodium salt (uranin) and stilbene 420 (S420) are for the red, green, and blue emissions, respectively (Fig. 9b). When the excitation energy exceeded their thresholds, strong laser emissions were observed with peaks at 425, 555, and 606 nm, respectively. The linewidth of each laser mode is as narrow as ~0.3 nm. By adjusting the excitation, any combination of two or three colors of laser emission can be obtained. For example, RGB laser pixels are achieved synchronously when spherical caps of three colors are excited simultaneously. Fig. 9c presents the calculated chromaticity of these laser spectra on the CIE1931 color diagram. The printed RGB pixel can cover 45% more perceptible colors than the standard RGB space. The wider color gamut indicates the advantages of printed RGB microlaser arrays in producing displays with excellent color saturation. Combined with the programmable excitation control system, the display of color images can be achieved. For example, Fig. 9d–f demonstrates an image of a butterfly using a full-color laser display with a 44 × 44 pixel array. This work demonstrates the printed microlaser arrays using organic semiconductor materials and their applicability for self-emitting full-color laser displays.

6. Conclusion and outlook

In conclusion, organic micro-nanocrystals constructed relying on intermolecular interactions have the characteristics of easy preparation[97,98] and few intrinsic defects and are considered to be one of the best choices for revealing the intrinsic properties of materials and building high-performance optoelectronic devices, which have aroused great interest of researchers. In this review, we provide an overview of the research progress of organic micro/nanocrystal lasers, including the potential impact of molecular aggregate modes on the morphology of organic micro/nanocrystals, the characteristics and research status of lasing in different mode resonators, crystal preparation methods and crystal array lasers in photonic applications.[99–101] The controllable and efficient preparation of organic crystals with tunable morphology and optical properties is still a challenge.

First of all, a variety of gain materials have been reported, such as organic small molecule materials, polymer materials, and MOF systems, which can cover a wide spectrum from ultraviolet to near-infrared, and the threshold is also as low as the μJ cm^{-2}. In the following, we elucidate the relationship between molecular arrangement and crystal morphology and introduce three typical optical resonator modes with various crystal morphologies, such as FP, WGM, and ring resonators. We introduce three typical optical resonator modes with various crystal morphologies, such as FP, WGM, and ring resonators. Organic crystal lasers have been used in many fields, such as display, information security, biological imaging, and vapor sensing. In addition, the preparation of large-area organic crystal arrays with precisely controlled orientation is of great significance in the preparation and integration of high-performance optoelectronic devices. We focus on the development of crystal laser arrays and their applications in optical devices. The patterned laser arrays demonstrate the feasibility of organic micro/nanocrystal lasers for novel multifunctional integrated circuit applications.[102]

Despite the many successes that have been achieved in the field of organic crystal lasers, the field still faces many challenges. First, the relationship between molecular structures/aggregation modes and micro/nanocrystal morphology and optical properties needs further studies to be established precisely and quantitatively. In addition, the current development of organic crystal laser is only in the stage of optical laser, and it is necessary to explore the compatibility and integration of laser crystals and other functional material layers in the device. Second, electrically pumped organic lasers have broad application prospects because they do not require additional pump light sources and can further reduce costs. However, electrically pumped organic semiconductor lasers have not yet been

realized.[103–106] Combining the obtained research results and the reviews of other researchers, the following factors mainly restrict the development of electrically pumped organic lasers.[1,21,53,107] Organic electrically pumped lasers have high requirements on materials and device structures. The organic gain materials should simultaneously have characteristics of low optical loss, low threshold, distinguished thermal stability, and high charge carrier mobility. From the perspective of materials, it is necessary to overcome the contradiction between high charge mobility and high emission efficiency and design novel organic semiconductor materials with both properties. Secondly, the device structures with high efficiency and low loss at high current densities need to be designed.

The development of organic crystal lasers is still in the stage of vigorous development. It is believed that in the near future, with its superior and irreplaceable characteristics, it will shine in the field of semiconductor integrated circuits.

Conflicts of interest

There are no conflicts to declare.

Acknowledgements

The authors acknowledge the financial support from the National Natural Science Foundation of China (no. 21971185, 52173177), the Natural Science Foundation of Jiangsu Province (no. BK20221362), and the Science and Technology Support Program of Jiangsu Province (no. TJ-2022-002). Furthermore, this work is supported by the Suzhou Key Laboratory of Functional Nano & Soft Materials, Collaborative Innovation Center of Suzhou Nano Science & Technology, the 111 Project, the Joint International Research Laboratory of Carbon-Based Functional Materials and Devices, and Soochow University Tang Scholar.

References

1 Y. Jiang, Y. Y. Liu, X. Liu, H. Lin, K. Gao, W. Y. Lai and W. Huang, Organic solid-state lasers: a materials view and future development, *Chem. Soc. Rev.*, 2020, **49**, 5885.
2 T. H. Maiman, Stimulated optical radiation in Ruby, *Nature*, 1960, **187**, 493.
3 F. H. Nicoll, Ultraviolet ZnO laser pumped by an electron beam, *Appl. Phys. Lett.*, 1966, **9**, 13.
4 M. M. Stylianakis, T. Maksudov, A. Panagiotopoulos, G. Kakavelakis and K. Petridis, Inorganic and hybrid perovskite based laser devices: a review, *Materials*, 2019, **12**, 859.
5 D. Saxena, S. Mokkapati, P. Parkinson, N. Jiang, Q. Gao, H. H. Tan and C. Jagadish, Optically pumped room-temperature GaAs nanowire lasers, *Nat. Photonics*, 2013, **7**, 963.
6 S. Yakunin, L. Protesescu, F. Krieg, M. I. Bodnarchuk, G. Nedelcu, M. Humer, G. De Luca, M. Fiebig, W. Heiss and M. V. Kovalenko, Low-threshold amplified spontaneous emission and lasing from colloidal nanocrystals of caesium lead halide perovskites, *Nat. Commun.*, 2015, **6**, 8056.
7 C. Xu, J. Dai, G. Zhu, G. Zhu, Y. Lin, J. Li and Z. Shi, Whispering-gallery mode lasing in ZnO microcavities, *Laser Photonics Rev.*, 2014, **8**, 469.
8 S. Chu, G. Wang, W. Zhou, Y. Lin, L. Chernyak, J. Zhao, J. Kong, L. Li, J. Ren and J. Liu, Electrically pumped waveguide lasing from ZnO nanowires, *Nat. Nanotechnol.*, 2011, **6**, 506.
9 I. D. W. Samuel and G. A. Turnbull, Organic semiconductor lasers, *Chem. Rev.*, 2007, **107**, 1272.
10 G. Q. Wei, X. D. Wang and L. S. Liao, Recent advances in 1D organic solid-state lasers, *Adv. Funct. Mater.*, 2019, **29**, 1902981.
11 G. Q. Wei, X. D. Wang and L. S. Liao, Recent advances in organic whispering-gallery mode lasers, *Laser Photonics Rev.*, 2020, **14**, 2000257.
12 K. H. Kim, J. L. Liao, S. W. Lee, B. Sim, C. K. Moon, G. H. Lee, H. J. Kim, Y. Chi and J. J. Kim, Crystal organic light-emitting diodes with perfectly oriented non-doped Pt-based emitting layer, *Adv. Mater.*, 2016, **28**, 2526.
13 Z. Qin, H. Gao, H. Dong and W. Hu, Organic light-emitting transistors entering a new development stage, *Adv. Mater.*, 2021, **33**, e2007149.
14 C. Grivas and M. Pollnau, Organic solid-state integrated amplifiers and lasers, *Laser Photonics Rev.*, 2012, **6**, 419.
15 H. H. Fang, J. Yang, J. Feng, T. Yamao, S. Hotta and H. B. Sun, Functional organic single crystals for solid-state laser applications, *Laser Photonics Rev.*, 2014, **8**, 687.
16 X. Yang and B. Li, Laser emission from ring resonators formed by a quantum-dot-doped single polymer nanowire, *ACS Macro Lett.*, 2014, **3**, 1266.
17 S. Krämmer, F. Laye, F. Friedrich, C. Vannahme, C. L. C. Smith, A. C. Mendes, I. S. Chronakis, J. Lahann, A. Kristensen and H. Kalt, Electrospun polymer fiber lasers for applications in vapor sensing, *Adv. Opt. Mater.*, 2017, **5**, 1700248.
18 S. Kushida, D. Okada, F. Sasaki, Z. H. Lin, J. S. Huang and Y. Yamamoto, Low-threshold whispering gallery mode lasing from self-assembled microspheres of single-sort conjugated polymers, *Adv. Opt. Mater.*, 2017, **5**, 1700123.
19 X. Wang, Z. Z. Li, M. P. Zhuo, Y. Wu, S. Chen, J. Yao and H. Fu, Tunable near-infrared organic nanowire nanolasers, *Adv. Funct. Mater.*, 2017, **27**, 1703470.
20 Y. S. Zhao, A. Peng, H. Fu, Y. Ma and J. Yao, Nanowire waveguides and ultraviolet lasers based on small organic molecules, *Adv. Mater.*, 2008, **20**, 1661.
21 F. Matino, L. Persano, A. Camposeo and D. Pisignano, Laser systems and networks with organic nanowires and nanofibers, *Adv. Opt. Mater.*, 2019, **7**, 1900192.
22 Q. H. Cui, Y. S. Zhao and J. Yao, Photonic applications of one-dimensional organic single-crystalline nanostructures: optical waveguides and optically pumped lasers, *J. Mater. Chem.*, 2012, **22**, 4136.
23 Y. L. Shi, M. P. Zhuo, X. D. Wang and L. S. Liao, Two-dimensional organic semiconductor crystals for photonics applications, *ACS Appl. Nano Mater.*, 2020, **3**, 1080.

24 Y. S. Zhao, P. Zhan, J. Kim, C. Sun and J. X. Huang, Patterned growth of vertically aligned organic nanowire waveguide arrays, *ACS Nano*, 2010, **4**, 1630.
25 K. S. Park, B. Cho, J. Baek, J. K. Hwang, H. Lee and M. M. Sung, Single-crystal organic nanowire electronics by direct printing from molecular solutions, *Adv. Funct. Mater.*, 2013, **23**, 4776.
26 Y. Yan, C. Zhang, J. Yao and Y. S. Zhao, Recent advances in organic one-dimensional composite materials: design, construction, and photonic elements for information processing, *Adv. Mater.*, 2013, **25**, 3627.
27 Y. S. Zhao, H. Fu, A. Peng, Y. Ma, D. Xiao and J. Yao, Low-dimensional nanomaterials based on small organic molecules: preparation and optoelectronic properties, *Adv. Mater.*, 2008, **20**, 2859.
28 S. Chen, N. Chen, Y. L. Yan, T. Liu, Y. Yu, Y. Li, H. Liu, Y. S. Zhao and Y. Li, Controlling growth of molecular crystal aggregates for efficient optical waveguides, *Chem. Commun.*, 2012, **48**, 9011.
29 S. Y. Min, T. S. Kim, Y. Lee, H. Cho, W. Xu and T. W. Lee, Organic nanowire fabrication and device applications, *Small*, 2015, **11**, 45.
30 H. H. Fang, R. Ding, S. Y. Lu, Y. D. Yang, Q. D. Chen, J. Feng, Y. Z. Huang and H. B. Sun, Whispering-gallery mode lasing from patterned molecular single-crystalline microcavity array, *Laser Photonics Rev.*, 2013, **7**, 281.
31 X. Wang, Q. Liao, Q. Kong, Y. Zhang, Z. Xu, X. Lu and H. Fu, Whispering-gallery-mode microlaser based on self-assembled organic single-crystalline hexagonal microdisks, *Angew. Chem., Int. Ed.*, 2014, **53**, 5863.
32 X. Wang, H. Li, Y. Wu, Z. Xu and H. Fu, Tunable morphology of the self-assembled organic microcrystals for the efficient laser optical resonator by molecular modulation, *J. Am. Chem. Soc.*, 2014, **136**, 16602.
33 S. Varghese, S. K. Park, S. Casado, R. C. Fischer, R. Resel, B. Milian Medina, R. Wannemacher, S. Y. Park and J. Gierschner, Stimulated emission properties of sterically modified distyrylbenzene-based H-aggregate single crystals, *J. Phys. Chem. Lett.*, 2013, **4**, 1597.
34 C. Zhang, C. L. Zou, Y. Yan, R. Hao, F. W. Sun, Z. F. Han, Y. S. Zhao and J. Yao, Two-photon pumped lasing in single-crystal organic nanowire exciton polariton resonators, *J. Am. Chem. Soc.*, 2011, **133**, 7276.
35 Y. Lv, Z. Xiong, Y. Yao, A. Ren, S. Xiang, Y. S. Zhao and Z. Zhang, Controlled shape evolution of pure-MOF 1D microcrystals towards efficient waveguide and laser applications, *Chem. – Eur. J.*, 2021, **27**, 3297.
36 H. Mizuno, T. Maeda, H. Yanagi, H. Katsuki, M. Aresti, F. Quochi, M. Saba, A. Mura, G. Bongiovanni, F. Sasaki and S. Hotta, Optically pumped lasing from single crystals of a cyano-substituted thiophene/phenylene co-oligomer, *Adv. Opt. Mater*, 2014, **2**, 529.
37 C. Zhang, C. L. Zou, Y. Yan, C. Wei, J. M. Cui, F. W. Sun, J. Yao and Y. S. Zhao, Self-assembled organic crystalline microrings as active whispering-gallery-mode optical resonators, *Adv. Opt. Mater.*, 2013, **1**, 357.
38 W. Zhang, Y. Yan, J. Gu, J. Yao and Y. S. Zhao, Low-threshold wavelength-switchable organic nanowire lasers based on excited-state intramolecular proton transfer, *Angew. Chem., Int. Ed.*, 2015, **54**, 7125.
39 C. Wei, S. Y. Liu, C. L. Zou, Y. Liu, J. Yao and Y. S. Zhao, Controlled self-assembly of organic composite microdisks for efficient output coupling of whispering-gallery-mode lasers, *J. Am. Chem. Soc.*, 2015, **137**, 62.
40 S. Z. Bisri, K. Sawabe, M. Imakawa, K. Maruyama, T. Yamao, S. Hotta, Y. Iwasa and T. Takenobu, Organic single-crystal light-emitting transistor coupling with optical feedback resonators, *Sci. Rep.*, 2012, **2**, 985.
41 Z. Yu, Y. Wu, Q. Liao, H. Zhang, S. Bai, H. Li, Z. Xu, C. Sun, X. Wang, J. Yao and H. Fu, Self-assembled microdisk lasers of perylenediimides, *J. Am. Chem. Soc.*, 2015, **137**, 15105.
42 Z. Gao, B. Xu, Y. Fan, T. Zhang, S. Chen, S. Yang, W. Zhang, X. Sun, Y. Wei, Z. Wang, X. Wang, X. Meng and Y. S. Zhao, Topological-distortion-driven amorphous spherical metal-organic frameworks for high-quality single-mode microlasers, *Angew. Chem., Int. Ed.*, 2021, **60**, 6362.
43 Y. Lv, X. Xiong, Y. Liu, J. Yao, Y. J. Li and Y. S. Zhao, Gallery-mode lasers based on self-assembled organic single-crystalline microrings, *Nano Lett.*, 2019, **19**, 1098.
44 Z. Yu, Y. Wu, L. Xiao, J. Chen, Q. Liao, J. Yao and H. Fu, Organic phosphorescence nanowire lasers, *J. Am. Chem. Soc.*, 2017, **139**, 6376.
45 X. Wang, Q. Liao, X. Lu, H. Li, Z. Xu and H. Fu, Shape-engineering of self-assembled organic single microcrystal as optical microresonator for laser applications, *Sci. Rep.*, 2014, **4**, 7011.
46 M. P. Zhuo, Y. X. Zhang, Z. Z. Li, Y. L. Shi, X. D. Wang and L. S. Liao, Controlled synthesis of organic single-crystalline nanowires via the synergy approach of the bottom-up/top-down processes, *Nanoscale*, 2018, **10**, 5140.
47 H. Huang, Z. Yu, D. Zhou, S. Li, L. Fu, Y. Wu, C. Gu, Q. Liao and H. Fu, Wavelength-turnable organic microring laser arrays from thermally activated delayed fluorescent emitters, *ACS Photonics*, 2019, **6**, 3208.
48 S. M. Yoon, J. Lee, J. H. Je, H. C. Choi and M. Yoon, Optical waveguiding and lasing action in porphyrin rectangular microtube with subwavelength wall thicknesses, *ACS Nano*, 2011, **5**, 2923.
49 X. Wang, Q. Liao, H. Li, S. Bai, Y. Wu, X. Lu, H. Hu, Q. Shi and H. Fu, Near-infrared lasing from small-molecule organic hemispheres, *J. Am. Chem. Soc.*, 2015, **137**, 9289.
50 Y. Liu, H. Dong, K. Wang, Z. Gao, C. Zhang, X. Liu, Y. S. Zhao and F. Hu, Suppressing nonradiative processes of organic dye with metal-organic framework encapsulation toward near-infrared solid-state microlasers, *ACS Appl. Mater. Interfaces*, 2018, **10**, 35455.
51 J. J. Wu, M. P. Zhuo, R. Lai, S. N. Zou, C. C. Yan, Y. Yuan, S. Y. Yang, G. Q. Wei, X. D. Wang and L. S. Liao, Cascaded excited-state intramolecular proton transfer towards near-infrared organic lasers beyond 850 nm, *Angew. Chem., Int. Ed.*, 2021, **60**, 9114.
52 J. J. Wu, X. D. Wang and L. S. Liao, Advances in energy-level systems of organic lasers, *Laser Photonics Rev.*, 2022, **16**, 2200366.

53 Y. Ma, Z. Z. Li, H. Lin, S. Chen, S. Zhuo and X. D. Wang, Advances in organic micro/nanocrystals with tunable physicochemical properties, *Sci. China Mater.*, 2021, **65**, 593.
54 W. Yao, Y. Yan, L. Xue, C. Zhang, G. Li, Q. Zheng, Y. S. Zhao, H. Jiang and J. Yao, Controlling the structures and photonic properties of organic nanomaterials by molecular design, *Angew. Chem., Int. Ed.*, 2013, **52**, 8713.
55 C. F. Xu, Y. Yu, Q. Lv, C. C. Yan, X. D. Wang and L. S. Liao, Rational self-assembly of polygonal organic microcrystals for shape-dependent multi-directional 2D optical waveguides, *Chin. Chem. Lett.*, 2022, **33**, 3255.
56 L. T. Kang, Z. C. Wang, Z. W. Cao, Y. Ma, H. B. Fu and J. N. Yao, Colloid chemical reaction route to the preparation of nearly monodispersed perylene nanoparticles: size-tunable synthesis and three-dimensional self-organization, *J. Am. Chem. Soc.*, 2007, **129**, 7305.
57 Z. Luo, Y. Liu, L. Kang, Y. Wang, H. Fu, Y. Ma, J. Yao and B. H. Loo, Controllable nanonet assembly utilizing a pressure-difference method based on anodic aluminum oxide templates, *Angew. Chem., Int. Ed.*, 2008, **47**, 8905.
58 X. Zhang, C. Dong, J. A. Zapien, S. Ismathullakhan, Z. Kang, J. Jie, X. Zhang, J. C. Chang, C. S. Lee and S. T. Lee, Polyhedral organic microcrystals: from cubes to rhombic dodecahedra, *Angew. Chem., Int. Ed.*, 2009, **48**, 9121.
59 M. P. Zhuo, Y. C. Tao, X. D. Wang, S. Chen and L. S. Liao, Rational synthesis of organic single-crystalline microrods and microtubes for efficient optical waveguides, *J. Mater. Chem. C*, 2018, **6**, 9594.
60 K. Liu, K. Huang, A. Lv, W. Ye, Y. Yang, K. Shen, J. Zhi, H. Wang, R. Zhang, J. Wang, H. Ma, H. Shi, W. Yao, Z. An and W. Huang, Tunable microstructures of ultralong organic phosphorescence materials, *Chem. Commun.*, 2021, **57**, 7276.
61 N. Tessler, G. J. Denton and R. H. Friend, Lasing from conjugated-polymer microcavities, *Nature*, 1996, **382**, 695.
62 Y. S. Zhao, H. Fu, A. Peng, Y. Ma, Q. Liao and J. Yao, Construction and optoelectronic properties of organic one-dimensional nanostructures, *Acc. Chem. Res.*, 2010, **43**, 409.
63 N. Pourdavoud, A. Mayer, M. Buchmüller, K. Brinkmann, T. Häger, T. Hu, R. Heiderhoff, I. Shutsko, P. Görrn, Y. Chen, H. C. Scheer and T. Riedl, Distributed feedback lasers based on $MAPbBr_3$, *Adv. Mater. Technol.*, 2018, **3**, 1700253.
64 J. A. Rogers, M. Meier and A. Dodabalapur, Using printing and molding techniques to produce distributed feedback and Bragg reflector resonators for plastic lasers, *Appl. Phys. Lett.*, 1998, **73**, 1766.
65 M. Rashidi, T. Haggren, Z. Su, C. Jagadish, S. Mokkapati and H. H. Tan, Managing resonant and nonresonant lasing modes in gaas nanowire random lasers, *Nano Lett.*, 2021, **21**, 3901.
66 S. Kim, S. Yang, S. H. Choi, Y. L. Kim, W. Ryu and C. Joo, Random lasing from structurally-modulated silk fibroin nanofibers, *Sci. Rep.*, 2017, **7**, 4506.
67 H. Dong, C. Zhang, F. J. Shu, C. L. Zou, Y. Yan, J. Yao and Y. S. Zhao, Superkinetic growth of oval organic semiconductor microcrystals for chaotic lasing, *Adv. Mater.*, 2021, **33**, e2100484.
68 J. Yu, Y. Cui, H. Xu, Y. Yang, Z. Wang, B. Chen and G. Qian, Confinement of pyridinium hemicyanine dye within an anionic metal-organic framework for two-photon-pumped lasing, *Nat. Commun.*, 2013, **4**, 2719.
69 L. He, Ş. K. Özdemir and L. Yang, Whispering gallery microcavity lasers, *Laser Photonics Rev.*, 2013, **7**, 60.
70 K. Hirose, Y. Liang, Y. Kurosaka, A. Watanabe, T. Sugiyama and S. Noda, Watt-class high-power, high-beam-quality photonic-crystal lasers, *Nat. Photonics*, 2014, **8**, 406.
71 S. Strauf, K. Hennessy, M. T. Rakher, Y. S. Choi, A. Badolato, L. C. Andreani, E. L. Hu, P. M. Petroff and D. Bouwmeester, Self-tuned quantum dot gain in photonic crystal lasers, *Phys. Rev. Lett.*, 2006, **96**, 127404.
72 C. H. Zhang, C. L. Zou, H. Y. Dong, Y. L. Yan, J. N. Yao and Y. S. Zhao, Dual-color single-mode lasing in axially coupled organic nanowire resonators, *Sci. Adv.*, 2017, **3**, 1700225.
73 K. Takazawa, J. Inoue, K. Mitsuishi and T. Takamasu, Fraction of a millimeter propagation of exciton polaritons in photoexcited nanofibers of organic dye, *Phys. Rev. Lett.*, 2010, **105**, 067401.
74 C. G. B. Garrett, W. Kaiser and W. L. Bond, Stimulated emission into optical whispering modes of spheres, *Phys. Rev.*, 1961, **124**, 1807.
75 H. Dong, C. Zhang, X. Lin, Z. Zhou, J. Yao and Y. S. Zhao, Dual-wavelength switchable vibronic lasing in single-crystal organic microdisks, *Nano Lett.*, 2017, **17**, 91.
76 Y. C. Tao, X. D. Wang and L. S. Liao, Active whispering-gallery-mode optical microcavity based on self-assembled organic microspheres, *J. Mater. Chem. C*, 2019, **7**, 3443.
77 J. Zhao, Y. Yan, Z. Gao, Y. Du, H. Dong, J. Yao and Y. S. Zhao, Full-color laser displays based on organic printed microlaser arrays, *Nat. Commun.*, 2019, **10**, 870.
78 Y. Du, C. L. Zou, C. Zhang, K. Wang, C. Qiao, J. Yao and Y. S. Zhao, Tuneable red, green, and blue single-mode lasing in heterogeneously coupled organic spherical microcavities, *Light: Sci. Appl.*, 2020, **9**, 151.
79 C. Wei, Y. Du, Y. Liu, X. Lin, C. Zhang, J. Yao and Y. S. Zhao, Organic janus microspheres: a general approach to all-color dual-wavelength microlasers, *J. Am. Chem. Soc.*, 2019, **141**, 5116.
80 C. Wei, M. Gao, F. Hu, J. Yao and Y. S. Zhao, Excimer emission in self-assembled organic spherical microstructures: an effective approach to wavelength switchable microlasers, *Adv. Opt. Mater.*, 2016, **4**, 1009.
81 N. Chandrasekhar and R. Chandrasekar, Reversibly shape-shifting organic optical waveguides: formation of organic nanorings, nanotubes, and nanosheets, *Angew. Chem., Int. Ed.*, 2012, **51**, 3556.
82 A. J. C. Kuehne and M. C. Gather, Organic lasers: recent developments on materials, device geometries, and fabrication techniques, *Chem. Rev.*, 2016, **116**, 12823.
83 C. Feng, Z. Xu, X. Wang, H. Yang, L. Zheng and H. Fu, Organic-nanowire-SiO_2 core-shell microlasers with highly polarized and narrow emissions for biological imaging, *ACS Appl. Mater. Interfaces*, 2017, **9**, 7385.
84 J. Xu, C. Peng, M. Yu and J. Zheng, Renal clearable noble metal nanoparticles: photoluminescence, elimination, and

biomedical applications, *Wiley Interdiscip. Rev.: Nanomed. Nanobiotechnol.*, 2017, **9**, 1453.
85 Y. L. Shi and X. D. Wang, 1D organic micro/nanostructures for photonics, *Adv. Funct. Mater.*, 2020, **31**, 2008149.
86 J. Feng, X. Jiang, X. Yan, Y. Wu, B. Su, H. Fu, J. Yao and L. Jiang, ''Capillary-Bridge Lithography'' for Patterning Organic Crystals toward Mode-Tunable Microlaser Arrays, *Adv. Mater.*, 2017, **29**, 1603652.
87 J. Feng, W. Wen, X. Wei, X. Jiang, M. Cao, X. Wang, X. Zhang, L. Jiang and Y. Wu, Random organic nanolaser arrays for cryptographic primitives, *Adv. Mater.*, 2019, **31**, e1807880.
88 C. Herder, M. D. Yu, F. Koushanfar and S. Devadas, Physical unclonable functions and applications: a tutorial, *Proc. IEEE Inst. Electr. Electron. Eng.*, 2014, **102**, 1126.
89 R. Pappu, B. Recht, J. Taylor and N. Gershenfeld, Physical one-way functions, *Science*, 2002, **297**, 2026.
90 R. Horstmeyer, B. Judkewitz, I. M. Vellekoop, S. Assawaworrarit and C. Yang, Physical key-protected one-time pad, *Sci. Rep.*, 2013, **3**, 3543.
91 J. J. Wu, H. Gao, R. Lai, M. P. Zhuo, J. Feng, X. D. Wang, Y. Wu, L. S. Liao and L. Jiang, Near-infrared organic single-crystal nanolaser arrays activated by excited-state intramolecular proton transfer, *Matter*, 2020, **2**, 1233.
92 X. Zhan, F. F. Xu, Z. Zhou, Y. Yan, J. Yao and Y. S. Zhao, 3D laser displays based on circularly polarized lasing from cholesteric liquid crystal arrays, *Adv. Mater.*, 2021, **33**, e2104418.
93 S. Liao, Z. Yang, J. Lin, S. Wang, J. Zhu, S. Chen, F. Huang, Y. Zheng and D. Chen, Hierarchical structure perovskite quantum dots film for laser-driven projection display, *Adv. Funct. Mater.*, 2022, **33**, 2210558.
94 F. F. Xu, Y. J. Li, Y. Lv, H. Dong, X. Lin, K. Wang, J. Yao and Y. S. Zhao, Flat-panel laser displays based on liquid crystal microlaser arrays, *CCS Chem.*, 2020, **2**, 369.
95 J. B. Wright, S. Liu, G. T. Wang, Q. Li, A. Benz, D. D. Koleske, P. Lu, H. Xu, L. Lester, T. S. Luk, I. Brener and G. Subramania, Multi-colour nanowire photonic crystal laser pixels, *Sci. Rep.*, 2013, **3**, 2982.
96 K. V. Chellappan, E. Erden and H. Urey, Laser-based displays: a review, *Appl. Opt.*, 2010, **49**, 79.
97 Z. Qi, B. Zhou and D. Yan, Recent Advances on Molecule-Based Micro/Nanocrystal Heterojunctions for Optical Applications. *Adv*, *Opt. Mater.*, 2022, **11**, 2200852.
98 S. Wu, B. Zhou and D. Yan, Recent advances on molecular crystalline luminescent materials for optical waveguides, *Adv. Opt. Mater.*, 2021, **10**, 2001768.
99 D. Yan, H. Yang, Q. Meng, H. Lin and M. Wei, Two-component molecular materials of 2,5-diphenyloxazole exhibiting tunable ultraviolet/blue polarized emission, pump-enhanced luminescence, and mechanochromic response, *Adv. Funct. Mater.*, 2014, **24**, 587.
100 D. Yan, W. Jones, G. Fan, M. Wei and D. G. Evans, Organic microbelt array based on hydrogen-bond architecture showing polarized fluorescence and two-photon emission, *J. Mater. Chem. C*, 2013, **1**, 4138.
101 S. Li, Y. Hao, S. Guo, C. Ding, Y. Ma, R. Liu and D. Yan, Three-primary-color molecular cocrystals showing white-light luminescence, tunable optical waveguide and ultra-high polarized emission, *Sci. China: Chem.*, 2022, **65**, 408.
102 C. Qiao, C. Zhang, Z. Zhou, J. Yao and Y. S. Zhao, An optically reconfigurable Förster resonance energy transfer process for broadband switchable organic single-mode microlasers, *CCS Chem.*, 2022, **4**, 250.
103 Q. Zhang, W. Tao, J. Huang, R. Xia and J. Cabanillas Gonzalez, Toward electrically pumped organic lasers: a review and outlook on material developments and resonator architectures, *Adv. Photonics Res.*, 2021, **2**, 2000155.
104 S. Z. Bisri, T. Takenobu and Y. Iwasa, The pursuit of electrically-driven organic semiconductor lasers, *J. Mater. Chem. C*, 2014, **2**, 2827.
105 M. Alipour and S. Damiri, Excited-state properties of organic semiconductor dyes as electrically pumped lasing candidates from new optimally tuned range-separated models, *Phys. Chem. Chem. Phys.*, 2022, **24**, 8003.
106 M. A. Baldo, R. J. Holmes and S. R. Forrest, Prospects for electrically pumped organic lasers, *Phys. Rev. B: Condens. Matter Mater. Phys.*, 2002, **66**, 035321.
107 K. Wang and Y. S. Zhao, Pursuing electrically pumped lasing with organic semiconductors, *Chem*, 2021 **7**, 3221.

